Additive Manufacturing Frontiers 3 (2024) 200132

Contents lists available at ScienceDirect

Additive Manufacturing Frontiers

journal homepage: www.elsevier.com/locate/amf

Microstructure and Phase Transformation Behavior of NiTiCu Shape Memory Alloys Produced Using Twin-Wire Arc Additive Manufacturing

Long Chen[a], João Pedro Oliveira[b], Xi Yan[a], Bowen Pang[a], Wenchao Ke[a], Jiajia Shen[b,c], Fissha Biruke Teshome[a], Norbert Schell[d], Naixun Zhou[a], Bei Peng[a], Zhi Zeng[a,e,*]

[a] School of Mechanical and Electrical Engineering, University of Electronic Science and Technology of China, Chengdu, 611731, China
[b] CENIMAT/I3N, Department of Materials Science, NOVA School of Science and Technology, Universidade NOVA de Lisboa, Caparica, 2829-516, Portugal
[c] UNIDEMI, Department of Mechanical and Industrial Engineering, NOVA School of Science and Technology, Universidade NOVA de Lisboa, Caparica, 2829-516, Portugal
[d] Institute of Materials Physics, Helmholtz-Zentrum Hereon, Max-Planck-Str. 1, Geesthacht, D-21502, Germany
[e] Institute of Electronic and Information Engineering, University of Electronic Science and Technology of China, Dongguan, 523808, China

ARTICLE INFO

Keywords:
Twin-wire arc additive manufacturing
Niticu alloys
Microstructure
Phase transformation
Synchrotron radiation

ABSTRACT

NiTiCu thin walls were produced by twin-wire arc additive manufacturing (T-WAAM) using commercial NiTi and Cu wires as the feedstock materials. This approach aims to solve the problems typically associated with large phase transformation hysteresis in NiTi shape memory alloys. The microstructure, mechanical properties, and phase transformation behavior of the as-deposited NiTiCu alloy were comprehensively examined. The results revealed that the as-deposited NiTiCu alloy was well-formed, with its microstructure showed columnar, equiaxed, and needle-like grains, depending on the location within the deposited walls. The microhardness gradually increased from the first to the third layer. The Cu content was 20.80 at%, and Cu-based precipitates were formed in the as-deposited NiTiCu. The volume fractions and lattice parameters of the matrix and precipitates in the as-deposited NiTiCu material were analyzed using high-energy synchrotron X-ray diffraction. The martensitic phase was identified as a B19 crystal structure, and the as-deposited NiTiCu underwent a one-step B2-B19 phase transformation. The tensile strength and fracture strain were approximately 232 MPa and 3.72%, respectively. In particular, the addition of Cu narrowed the phase transformation hysteresis of the as-deposited NiTiCu alloy from 24.4 to 7.1 °C compared with conventional binary NiTi alloys. This study expands the potential of T-WAAM in modifying the phase transformation behavior of NiTi-based ternary alloys.

1. Introduction

NiTi-based shape memory alloys (SMAs) exhibit remarkable properties, including shape memory effect, superelasticity, excellent biocompatibility, and high corrosion resistance. These properties make them useful in diverse fields, such as aerospace, automotive, biomedicine, and intelligent manufacturing [1–3]. However, commercial binary NiTi alloys have low phase transformation temperatures and large phase transformation hysteresis, which limit their application in environments susceptible to significant thermal alternations [4]. Introducing a third element into NiTi alloys is effective for manipulating the phase transformation temperature and hysteresis [5]. In particular, the addition of Cu can effectively narrow the phase transformation hysteresis and improve the thermal stability of NiTiCu alloy systems via alloy substitution, promoting the application of NiTiCu alloys in temperature-sensitive sensors and actuators [6–8]. Nonetheless, it is difficult to accurately adjust the atomic composition ratio of NiTi-based alloys during traditional manufacturing processes, such as casting and powder metallurgy, as this material system easily absorbs impurities that make the alloy brittle [9,10]. In addition, traditional manufacturing methods have limitations in the formation of NiTi-based alloys with complex shapes [11], which limits their widespread use.

Additive manufacturing (AM) technologies, which serve as near-net shape manufacturing methods, enable the production of complex-shaped parts using a layer-by-layer deposition approach, effectively overcoming the shortcomings of traditional manufacturing [12]. Laser powder bed fusion (LPBF) is the most widely used AM process for fabricating NiTi-based alloys. The phase transformation temperatures can be regulated, cracking and porosity defects can be minimized, and the mechanical properties can be improved by optimizing the LPBF processing parameters [13–15]. However, LPBF is limited by the part size, preparation costs, and manufacturing efficiency.

* Corresponding author.
E-mail address: zhizeng@uestc.edu.cn (Z. Zeng).

https://doi.org/10.1016/j.amf.2024.200132
Received 18 September 2023; Received in revised form 28 November 2023; Accepted 14 December 2023
Available online 29 March 2024

Table 1
Elemental composition (wt%) of NiTi and Cu wires and TA1 substrate.

Materials	Composition (wt%)								
	Ni	Ti	Cu	Sn	Mn	Si	Fe	C	O
NiTi wire	55.62	Bal.	–	–	–	–	0.007	0.007	0.0342
Cu wire	–	–	Bal.	0.93	0.38	0.12	–	–	–
TA1 substrate	–	Bal.	–	–	–	0.1	0.15	0.05	0.15

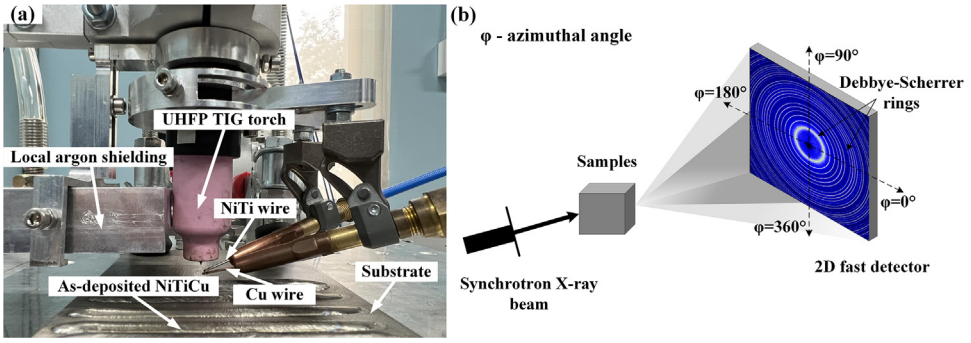

Fig. 1. Experimental methods: (a) Setup for T-WAAM process; (b) Schematic representation of SXRD experiment.

Wire arc AM (WAAM) uses an electric arc as the heat source and a solid wire as the feedstock material. WAAM has several advantages, such as high deposition speed, low defect level, and low preparation costs [16]. Wang et al. [17] successfully fabricated Ni-rich NiTi alloys using Ni and Ti wires via WAAM with a tungsten inert gas (TIG) heat source. The effects of deposition current and substrate heating temperature on the crystallographic orientation, precipitation, phase transformation, and mechanical properties of WAAM for NiTi alloys were subsequently investigated [18,19]. Furthermore, by introducing an ultra-high frequency pulse (UHFP) during TIG-assisted WAAM, Zeng et al. [20] fabricated a NiTi thin wall using a commercial Ni-rich NiTi wire, which exhibited an austenite state at room temperature and superelastic behavior. In addition, twin-WAAM (T-WAAM), which involves the use of two independent solid wires during WAAM, has been proven to effectively control the atomic composition ratio of NiTi alloys by setting different wire feed speeds [21].

In this study, NiTiCu SMAs with narrow phase transformation hysteresis were manufactured by T-WAAM using NiTi and Cu wires as feedstock materials. The microstructure, mechanical properties, and chemical composition of as-deposited NiTiCu were characterized. Moreover, the existing phases and phase transformation behavior were revealed using high-energy synchrotron X-ray diffraction (SXRD) and differential scanning calorimetry (DSC), respectively. This study provides insight into a new method for changing the phase transformation behavior of NiTi-based ternary SMAs using T-WAAM.

2. Experimental Procedures

Commercially available Φ1.0 mm Ni-rich NiTi and Cu wires were selected as feedstock materials for T-WAAM. A 200 mm × 100 mm × 15 mm TA1 titanium plate was used as the substrate. Table 1 lists the elemental compositions of the wires and substrates used in this study.

The T-WAAM setup mainly consisted of an ABB 1410 six-axis robot, a UHFP TIG torch, twin-wire feed nozzles, and an argon-shielding device, as shown in Fig. 1(a). The wire feed nozzles were positioned at 20° relative to the TA1 substrate surface with a horizontal angle of 60° between the twin-wire feed nozzles. In addition, lapping the NiTi wire on the Cu wire ensured adequate fusion and liquid bridge transition of the twin-wire droplets. The TA1 substrate was first preheated using direct current TIG to facilitate the subsequent deposition. The preheating current was 100 A, and the torch travel speed during the preheating stage was 100 mm/min. Ar gas (99.99%) was supplied at a flow rate of 15 L/min through the TIG torch and local shielding device to reduce oxidation. After preheating, a thin NiTiCu wall was deposited using T-WAAM with an UHFP TIG heat source. The processing parameters were optimized to achieve excellent forming quality, as listed in Table 2. Based on the wire feed speed ratio between the Cu and NiTi wires, the preset proportion of Cu in the as-deposited NiTiCu alloy was 20%.

Table 2
Processing parameters for T-WAAM with UHFP TIG.

Process parameters	Value
Base current (A)	100
UHFP current (A)	60
UHFP frequency (kHz)	20
UHFP duty cycle (%)	50
Arc length (mm)	3
Torch travel speed (mm/min)	300
NiTi wire feed speed (mm/min)	2200
Cu wire feed speed (mm/min)	240
Deposited time interval (min)	1

Cross-sectional specimens of as-deposited NiTiCu were cut vertically across the deposited layers. After grinding, polishing, and etching, the specimens were observed under a Nikon LV150 microscope for metallographic analysis. The polished specimens were analyzed using a JSM-7600F scanning electron microscope (SEM) coupled with energy dispersive spectroscopy (EDS) to determine their microstructures and chemical compositions. SXRD experiments were conducted at P07 High Energy Materials Science beamline of Petra III/ DESY to determine the existing phases in the as-deposited NiTiCu. A two-dimensional Perkin Elmer fast detector was used to capture the raw Debbye–Scherrer rings, as shown in Fig. 1(b). The wavelength selected for the experiment was 0.14235 Å. The distance between the sample and the detector was 1396 mm, as determined using LaB_6 calibration powder. The raw diffraction data were processed using a combination of Fit2D, Jade9, and MAUD [22]. The phase transformation behavior was analyzed using DSC214. The temperatures for the DSC measurements ranged from −100 to 120 °C, and the heating/cooling rate was 10 °C/min. Vickers microhardness was measured along the sample height using a Micro-586 microhardness tester with an indentation load of 4.9 N and a load duration of 10 s. Tensile samples, each with a length of 30 mm and thickness of 1 mm, were cut at the middle height of the as-deposited NiTiCu in a horizontal direction parallel to the substrate surface. An Instron 5548 micro-tensile testing

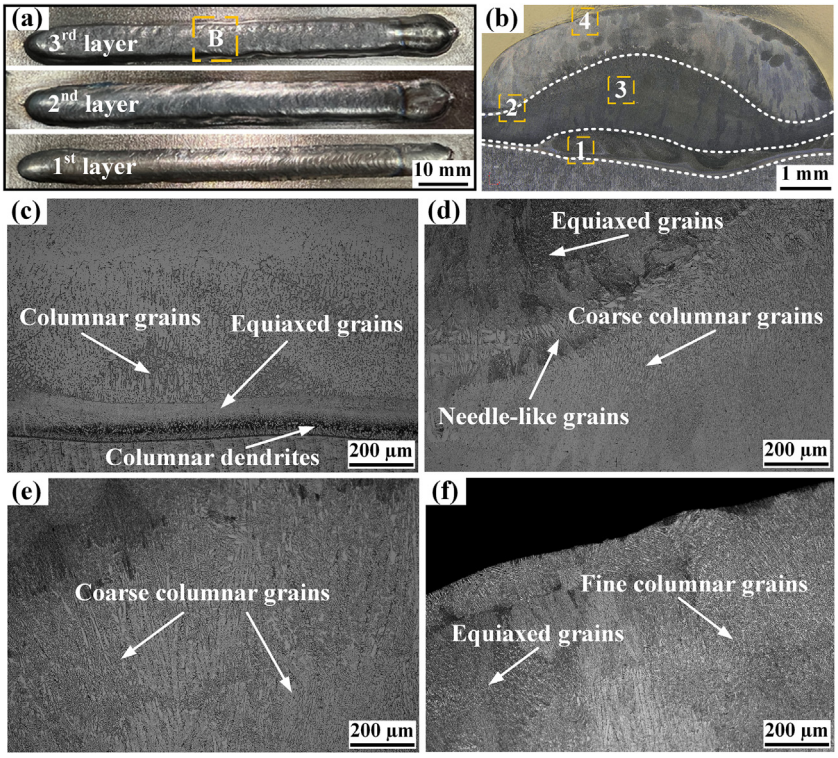

Fig. 2. Morphology of as-deposited NiTiCu: (a) Macroscopic morphology of different deposited layers; (b) Cross-section of zone B; Microstructure of (c) Region 1; (d) Region 2; (e) Region 3; (f) Region 4.

machine was used to continuously apply loads to the tensile samples at a displacement rate of 0.5 mm/min until fracturing occurred.

3. Results and Discussion

3.1. Microstructural characteristics and microhardness

Fig. 2(a) shows the details of the macroscopic morphology of the as-deposited NiTiCu, starting from the first to the third deposited layers. The deposited beads were continuous, with a steady morphology, uniform deposition width, and no defect. The cross-sectional specimen of zone B was free of cracks and porosity (Fig. 2(b)). An interlayer demarcation line was observed between each layer, indicating that remelting had occurred. Detailed microstructural characteristics for regions 1 – 4 are shown in Figs. 2(c – f). The first layer predominantly consisted of columnar grains (Fig. 2(c)). Columnar dendrites and equiaxed grains near the fusion line are related to the preheating and remelting effects of the first layer on the substrate. The remelting effect at high processing speeds resulted in the formation of finer grains [23,24]. Fig. 2(d) shows the fusion zone generated at the interface between the second and third deposited layers. Needle-like grains appeared at the fusion line, which is relevant to the epitaxial growth of the partially remelted grains. The microstructure of the second layer showed mainly coarse columnar grains (Fig. 2(e)). Because the second layer was reheated by the subsequent deposited layers, the columnar grains grew and became coarse [25]. The presence of fine columnar grains (Fig. 2(f)) is attributed to the absence of the time and temperature required for grain growth. The last layer did not experience any subsequent thermal cycling, which facilitated the appearance of equiaxed grains at this location.

The microhardness curve along the vertical centerline of the cross-section of the as-deposited NiTiCu, that is, in the direction of the deposited height, is shown in Fig. 3. The average microhardness values of the first, second, and third layers are approximately 320.9, 371.3, and 416.4 $HV_{0.5}$, respectively. The microhardness of the as-deposited NiTiCu gradually increased from the first to the third layers. The variation in microhardness is related to the different microstructures of the

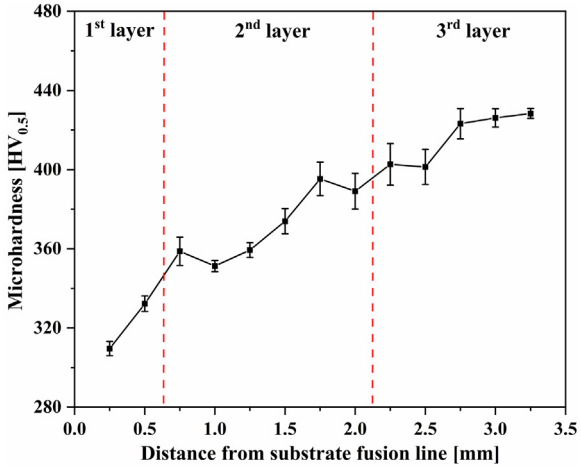

Fig. 3. Microhardness along vertical centerline of cross-section of as-deposited NiTiCu.

deposited layers [26,27]. The fine columnar grains in the top layer led to more grain boundaries and dislocations than the coarse columnar grains in the bottom layer, which was conducive for an increase in microhardness [25]. Simultaneously, the volume fraction and distribution of precipitates can result in microhardness transitions and fluctuations owing to the precipitation effect [17,21].

3.2. Chemical composition analysis

The microstructure in the center of the second deposited layer of the as-deposited NiTiCu was selected for chemical composition analysis, and the associated data are presented in Fig. 4, Fig. 5, and Table 3. The elemental distribution and atomic composition were obtained via EDS mapping, as shown in Fig. 4. The Ti, Ni, and Cu contents of the as-deposited NiTiCu were 44.33 at%, 34.86 at%, and 20.80 at%, respec-

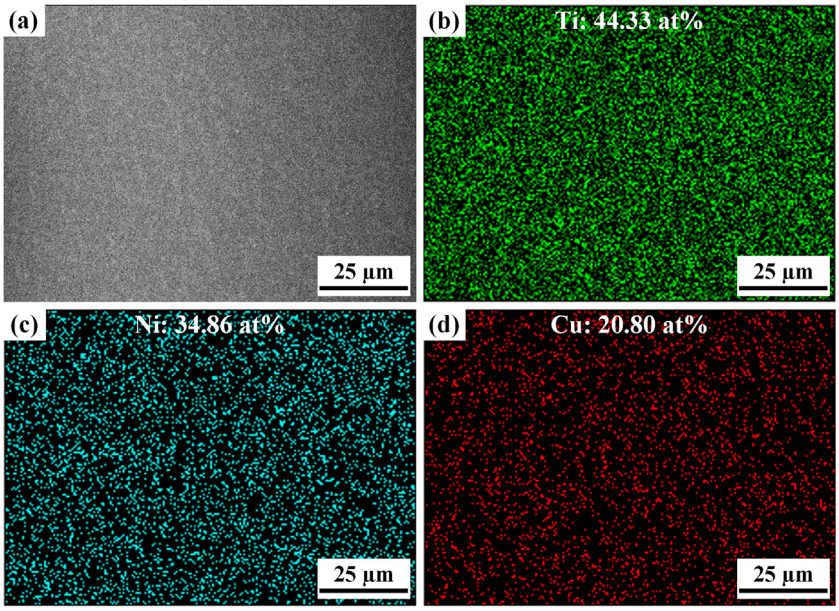

Fig. 4. Elemental distribution and atomic composition ratio of as-deposited NiTiCu: (a) EDS mapping; (b) Ti element; (c) Ni element; (d) Cu element.

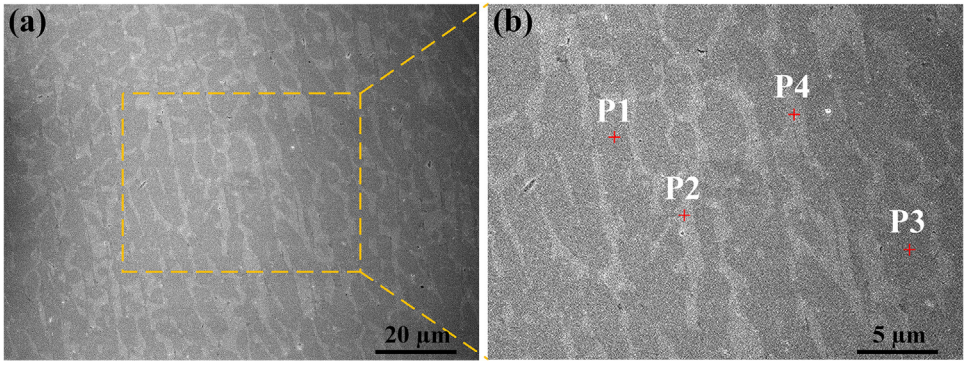

Fig. 5. SEM images and EDS point scanning positions of as-deposited NiTiCu: (a) Center of second deposited layer; (b) Point scanning locations.

Table 3
Results of EDS compositional analysis of points indicated in Fig. 5.

Points	Compositions (at%)			Possible phases
	Ni	Ti	Cu	
P1	39.5	48.9	11.6	NiTi, CuTi, Ti(Ni, Cu)
P2	29.4	39.5	31.0	NiTi, Cu_2Ti, Cu_3Ti, Ti(Ni, Cu)
P3	39.0	48.3	12.7	NiTi, CuTi, Ti(Ni, Cu)
P4	28.7	38.6	32.8	NiTi, Cu_2Ti, Cu_3Ti, Ti(Ni, Cu)

tively. The expected proportion of Cu was 20 at% based on the wire feed speed of twin wires. Therefore, the Cu contents obtained from the experiment and presetting were consistent.

Light gray coarse columnar grains were uniformly distributed on the dark gray matrix (Fig. 5), which is in good agreement with the microstructural analysis results. As listed in Table 3, the compositional ratios of the matrix at points P1 and P3 were similar, and the same results were obtained for the columnar grains at points P2 and P4, indicating that the elements were uniformly distributed in the as-deposited NiTiCu.

In addition, because the molar enthalpy of the formation of Ti-Cu is higher than that of Ti-Ni, the emergence of Ti-Cu phases had a weaker thermodynamic driving force [28]. Hence, Ti preferentially formed compounds with Ni, whereas the remaining Ti formed compounds with Cu. Because Cu and Ni can form a substitutional solid solution owing to their similarities in crystal structure, atomic radii, and electronegativity, Cu atoms can replace some Ni atoms in the material crystal structure. Moreover, the Cu content in the columnar grains was higher than that in the dark gray matrix. Therefore, the possible phases of the matrix might be NiTi, CuTi, Ti(Ni, Cu), and those of the columnar grains might contain NiTi, Cu_2Ti, Cu_3Ti, Ti(Ni, Cu) based on the compositional ratio of elements.

3.3. Phase analysis

Phase analysis was performed using SXRD to determine the phases in the as-deposited NiTiCu. A diffractogram of the NiTiCu sample after full integration along the azimuthal angle is shown in Fig. 6(a). The identified phases were B2, B19, CuTi, Cu_2Ti, and $Ti(Ni, Cu)_2$. These results were in good agreement with those of the EDS chemical composition analysis. No single Cu phase was detected in the SXRD results, indicating that sufficient in-situ alloying of Cu with NiTi occurred during the

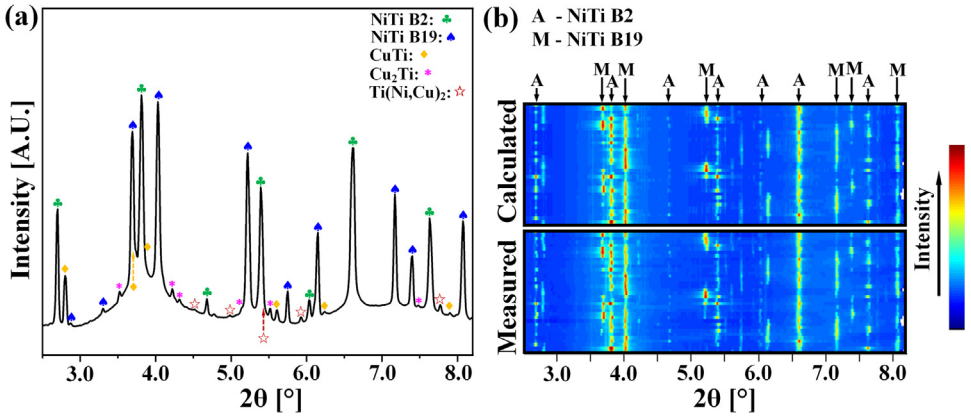

Fig. 6. SXRD pattern of as-deposited NiTiCu: (a) Diffractogram after full integration along azimuthal angle; (b) Rietveld refinement plot.

Table 4
Refined lattice parameters and volume fractions of all phases in as-deposited NiTiCu.

Phase	a (Å)	b (Å)	c (Å)	α (°)	β (°)	γ (°)	Volume fraction (%)
Matrix NiTi B2	3.022	$a = b = c$	$a = b = c$	90	90	90	57.9
Matrix NiTi B19	4.950	4.045	2.893	90	97.93	90	39.2
CuTi precipitates	3.107	$a = b$	2.906	90	90	90	1.35
Cu_2Ti precipitates	4.337	8.099	4.411	90	90	90	0.97
Ti(Ni, $Cu)_2$ precipitates	3.597	$a = b$	7.431	90	90	90	0.58

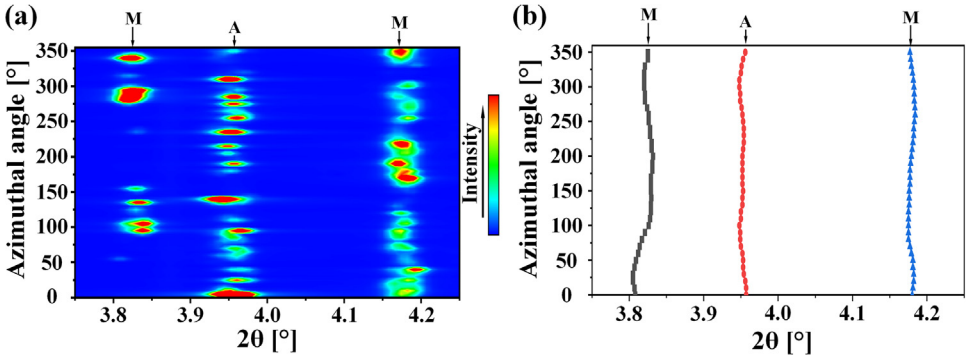

Fig. 7. Variations in diffraction peak with azimuthal angle and diffraction angle for austenite (A) and martensite (M) peaks: (a) Peak intensity; (b) Peak position.

T-WAAM process. In addition, the presence of Ti(Ni, $Cu)_2$ precipitates indicated that Cu replaced Ni to form this compound.

Rietveld refinement of the SXRD data was performed to quantify the volume fractions of all the phases and to determine the respective lattice parameters in the as-deposited NiTiCu. As shown in Fig. 6(b), good agreement was observed between the calculated and measured patterns after Rietveld refinement in terms of the position, width, and intensity, demonstrating a good fit. The peak positions of the precipitates are not marked in the refinement graph because of their relatively low intensities. The volume fractions and lattice parameters obtained from the calculations for all the phases are listed in Table 4. The volume fractions of matrix B2 and B19 phases were 57.9% and 39.2%, respectively, indicating the dominance of the B2 and B19 phases in the as-deposited NiTiCu. The volume fractions of CuTi, Cu_2Ti, and Ti(Ni, $Cu)_2$ precipitates were 1.35%, 0.91%, and 0.58%, respectively. Similar phase identification results were also described in Ref. [29], but were not quantified. The detection and quantification of low-volume-fraction phases in this study benefited from the high signal-to-noise ratio associated with SXRD.

The as-deposited NiTiCu texture was assessed qualitatively using contour maps of the diffraction peak intensity of two martensite and one austenite diffraction peaks for a 2θ range between 3.85° and 4.25°, as shown in Fig. 7(a). These diffraction peaks are typically adopted because they are isolated from other diffraction peaks and possess high diffraction intensities at most azimuthal angles, thereby preventing misidentification during peak fitting. The relationship between the peak position (displacement of the diffraction angle) and the azimuthal angle is represented in Cartesian coordinates, as shown in Fig. 7(b). The peak intensity and peak position shifted significantly with the azimuthal angle (Fig. 7), indicating the presence of a significant preferred orientation in the as-deposited NiTiCu, as typical during arc-based processing. The emergence of the preferred orientation was related to the relatively large grain size (coarse columnar grains) of the as-deposited NiTiCu. When these grains were diffracted at a specific azimuthal angle, very high diffraction intensities were observed.

Generally, the phases in NiTi alloys are mainly B2, B19′, and some Ti-Ni precipitates [30]. B19 and B19′ are martensitic phases with different lattice parameters. The martensitic lattice parameters of the as-deposited NiTiCu were relatively lower than those of other NiTi-based alloys [22,31], indicating that the martensitic structure of NiTiCu is significantly different from those of the others. Moreover, Nam et al. [32] mentioned that the B2-B19 phase transformation occurs in Ti-Ni-Cu alloys. Therefore, the martensitic phase in the NiTiCu alloy observed in this study was B19. In addition, pure Ti-Ni precipitates were not detected in the NiTiCu alloy; instead, Ti-Cu intermetallic compounds (IMCs) were observed. The microhardness of Ti-Cu IMCs is lower than that of Ti-Ni IMCs [33]. Therefore, the microhardness of the as-deposited NiTiCu was affected by the presence of Ti-Cu IMCs.

Table 5
Phase transformation temperatures and hysteresis of NiTi and NiTiCu alloys.

Materials	Transformation temperatures and hysteresis (°C)						
	M_s	M_f	M_p	A_s	A_f	A_p	A_p-M_p
NiTi wire	−25.2	−51.1	−35.5	−22.4	−2.2	−11.1	24.4
NiTiCu	52.8	28.3	46.7	42.1	60.2	53.8	7.1

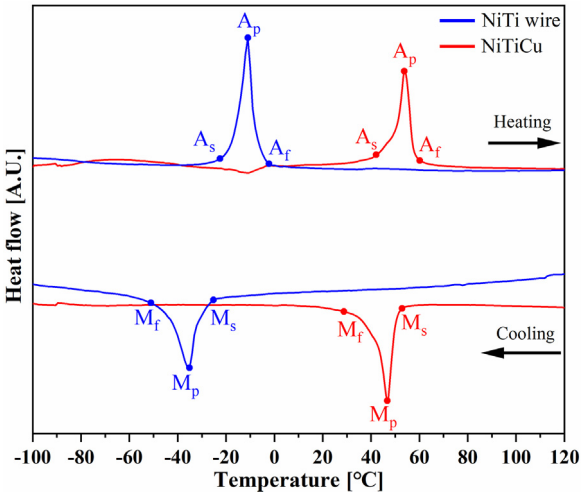

Fig. 8. DSC results of NiTi wire and as-deposited NiTiCu.

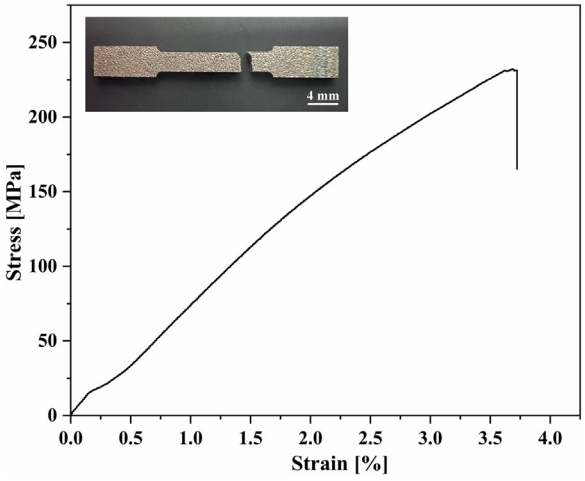

Fig. 9. Representative tensile stress–strain curve of as-deposited NiTiCu specimen.

3.4. Phase transformation behavior

The phase transformation behavior of the as-deposited NiTiCu was analyzed using DSC and compared with that of the NiTi wire feedstock. Fig. 8 shows the DSC results for the NiTi wire and as-deposited NiTiCu. The phase transformation temperatures and hystereses of both alloys are listed in Table 5. A_s, A_p, and A_f are the start, peak, and finish temperatures of the austenite phase transformation, respectively. M_s, M_p, and M_f are the start, peak, and finish temperatures of the martensite phase transformation, respectively.

The NiTiCu material underwent only a one-step phase transformation between high-temperature B2 and low-temperature B19 during the heating and cooling stages (Fig. 8). The phase transformation behavior of Ti-Ni-Cu alloys was closely related to the Cu content [34]. For example, when 1 at%–7 at% Cu was added, two-step or three-step phase transformations occurred, whereas a one-step phase transformation occurred at 10 at% Cu.

The M_s value of NiTiCu was 52.8 °C, whereas that of the NiTi wire was only −25.2 °C (Table 5). The M_s value of NiTiCu was 78 °C higher than that of NiTi, demonstrating that the addition of Cu increased the phase transformation temperature. The M_s value of NiTiCu alloy gradually increased with increasing Cu content, and even the addition of 1 at% Cu could significantly increase the M_s temperature [34]. The substitution of Ni with Cu and the subsequent formation of Ti-Cu IMCs decreased the Ni content in the matrix, further justifying the increased M_s value of the NiTiCu alloy [35]. In addition, the phase transformation hysteresis (A_p-M_p) of NiTiCu was 7.1 °C, whereas that of NiTi was 24.4 °C, indicating that the addition of Cu narrowed the phase transformation hysteresis of the NiTi alloy. In addition, the phase transformation hysteresis of NiTiCu alloys fabricated via laser-directed energy deposition (L-DED) varied between 11 and 17.2 °C [36,37]; in comparison, the phase transformation hysteresis of the NiTiCu alloys fabricated via T-WAAM was significantly narrower. This proves that T-WAAM is an effective AM method for preparing NiTiCu alloys with narrow phase transformation hysteresis.

3.5. Tensile properties

Conventional tensile fracture tests were performed at 25 °C to evaluate the mechanical properties of the as-deposited NiTiCu. A representative tensile stress–strain curve of the as-deposited NiTiCu specimen is shown in Fig. 9. The tensile strength of the as-deposited NiTiCu was 232 ± 11 MPa, and the corresponding fracture strain was 3.7% ± 0.7%. The fracture position of the tensile specimen was located in the parallel section of the specimen.

Compared with NiTiCu (Cu: 3 at% and 5 at%) alloys prepared via L-DED [36,37], the mechanical properties of the as-deposited NiTiCu prepared by T-WAAM deteriorated, which might be associated with the higher Cu content and the corresponding IMCs. The tensile strength and fracture strain of the NiTiCu alloys prepared by arc melting decreased significantly as the Cu content increased from 1 at% to 10 at% [34]. The same trend was observed for laser-welded NiTi-Cu alloys; the tensile strength reached its lowest value of approximately 176 MPa when the Cu content was 40 at% [38]. A comparison of the mechanical properties of the laser-welded joints with a Cu content of 20.7 at% (average tensile strength of approximately 280 MPa and fracture strain of approximately 3.2%) [33] shows that adding excess Cu can increase the fraction of Cu-rich brittle IMCs, leading to the deterioration of the mechanical properties [29].

In addition, the mechanical properties of NiTi-based alloys are influenced by the material transformation temperature, grain size, and precipitation. A generally negative relationship exists between the M_s temperature and critical stress [39]. Smaller grain sizes increase strength and elongation based on the Hall–Petch relationship [18]. Fine and uniform precipitates caused a strain-hardening effect that strengthens the material [40]. However, irregular and coarse precipitates are prone to crack initiation and propagation, resulting in decreased strength and ductility [41]. Therefore, measures to enhance the mechanical properties of the as-deposited NiTiCu must be improved in future studies.

4. Conclusions

NiTiCu alloys were successfully deposited using the T-WAAM technique. The microstructure, mechanical properties, and phase transformation behavior of the NiTiCu alloys were investigated. The following conclusions were drawn.

(1) The as-deposited NiTiCu alloy had a good forming quality, and its microstructure consisted of columnar, equiaxed, and needle-like grains, depending on the location within the deposited material. The microhardness gradually increased from the first to the third layer. The Cu content of the as-deposited material was 20.80 at%. The main phases were B2, B19, CuTi, Cu_2Ti, and $Ti(Ni, Cu)_2$, indicating that Cu reacted with Ti and replaced some Ni atoms. In-situ alloying of Cu with NiTi successfully occurred during T-WAAM.
(2) The dominance of the B2 and B19 phases in the as-deposited NiTiCu was determined based on the volume fractions quantified via Rietveld refinement using SXRD. The martensitic phase was found to be B19 based on the calculated lattice parameters. A significant preferred orientation in the as-deposited NiTiCu was developed owing to the solidification conditions typical of WAAM.
(3) The tensile strength and fracture strain of the as-deposited NiTiCu were 232 ± 11 MPa and 3.72% ± 0.7%, respectively. The as-deposited NiTiCu underwent only a one-step phase transformation between the high-temperature B2 and low-temperature B19 phases. Moreover, the as-deposited NiTiCu had a higher martensitic phase transformation temperature (M_s: 52.8 °C) and narrower phase transformation hysteresis (A_p-M_p=7.1 °C) than the NiTi wire (M_s=−25.2 °C, A_p-M_p= 24.4 °C).
(4) The feasibility of producing NiTiCu alloys with narrow phase transformation hysteresis using the T-WAAM technique was demonstrated, establishing a foundation for the efficient production of NiTi-based ternary SMAs using T-WAAM.

Declaration of competing interest

The authors declare that they have no known competing financial interests or personal relationships that may have influenced the work reported in this paper.

CRediT authorship contribution statement

Long Chen: Conceptualization, Investigation, Methodology, Validation, Writing – original draft. **João Pedro Oliveira:** Formal analysis, Resources, Writing – review & editing. **Xi Yan:** Data curation, Investigation. **Bowen Pang:** Data curation, Investigation. **Wenchao Ke:** Data curation, Investigation. **Jiajia Shen:** Data curation, Investigation. **Fissha Biruke Teshome:** Investigation. **Norbert Schell:** Investigation. **Naixun Zhou:** Data curation. **Bei Peng:** Project administration, Supervision. **Zhi Zeng:** Funding acquisition, Methodology, Project administration, Supervision.

Acknowledgments

This work was supported by National Natural Science Foundation of China (Grant No. 52175292), Science and Technology Project of Sichuan Province (Grant Nos. 23NSFJQ0064, 2022YFQ0058), and Guangdong Basic and Applied Basic Research Foundation (Grant No. 2021B1515140048). JPO and JS acknowledge the funding by national funds from Fundação para a Ciência e a Tecnologia (FCT), I.P., within the scope of projects LA/P/0037/2020, UIDP/50025/2020, and UIDB/50025/2020 of the Associate Laboratory Institute of Nanostructures, Nanomodelling, and Nanofabrication – i3N. The authors acknowledge DESY (Hamburg, Germany), a member of the Helmholtz Association HGF, for providing the experimental facilities. Part of this study was conducted at PETRA III. The research leading to this result was supported by project CALIPSOplus under Grant Agreement 730872 from the EU Framework Programme for Research and Innovation HORIZON 2020.

References

[1] Zhang YT, Attarilar S, Wang LQ, et al. A review on design and mechanical properties of additively manufactured NiTi implants for orthopedic applications. International Journal of Bioprinting 2021;7(2):15–42. doi:10.18063/ijb.v7i2.340.
[2] Wang X, Pu Z, Yang Q, et al. Improved functional stability of a coarse-grained Ti-50.8 at.% Ni shape memory alloy achieved by precipitation on dislocation networks. Scr Mater 2019;163:57–61. doi:10.1016/j.scriptamat.2019.01.006.
[3] Ou SF, Peng BY, Chen YC, et al. Manufacturing and characterization of NiTi alloy with functional properties by selective laser melting. Metals (Basel) 2018;8(5):342. doi:10.3390/met8050342.
[4] Singh N, Talapatra A, Junkaew A, et al. Effect of ternary additions to structural properties of NiTi alloys. Comput Mater Sci 2016;112:347–55. doi:10.1016/j.commatsci.2015.10.029.
[5] Zuo XD, Zhang W, Chen Y, et al. Wire-based directed energy deposition of NiTiTa shape memory alloys: Microstructure, phase transformation, electrochemistry, X-ray visibility and mechanical properties. Additive Manufacturing 2022;59:103115. doi:10.1016/j.addma.2022.103115.
[6] Apostol VD, Pricop B, Popa M, et al. The thermo-mechanical behavior of NiTi-X shape memory alloys. Mater Today: Proc 2023;72:572–5. doi:10.1016/j.matpr.2022.10.059.
[7] Qadir R, Mohammed S, KÖK M, et al. A review on NiTiCu shape memory alloys: Manufacturing and characterizations. Journal of Physical Chemistry and Functional Materials 2021;4(2):49–56. doi:10.54565/jphcfum.1018817.
[8] Yang C, Cheng QR, Liu LH, et al. Effect of minor Cu content on microstructure and mechanical property of NiTiCu bulk alloys fabricated by crystallization of metallic glass powder. Intermetallics 2015;56:37–43. doi:10.1016/j.intermet.2014.08.009.
[9] Kai WY, Chang KC, Wu HF, et al. Formation mechanism of Ni_2Ti_4Ox in NITI shape memory alloy. Materialia 2019;5:100194. doi:10.1016/j.mtla.2018.100194.
[10] Elahinia M, Moghaddam NS, Andani MT, et al. Fabrication of NiTi through additive manufacturing: A review. Prog Mater Sci 2016;83:630–63. doi:10.1016/j.pmatsci.2016.08.001.
[11] Polozov I, Popovich A. Microstructure and mechanical properties of NiTi-based eutectic shape memory alloy produced via selective laser melting in-situ alloying by Nb. Materials (Basel) 2021;14(10):2696. doi:10.3390/ma14102696.
[12] Lu B, Wang L. Development of additive manufacturing technology and industry in China. Chinese Journal of Engineering Science 2022;24(4):202–11. doi:10.15302/j-sscae-2022.04.018.
[13] Wang XB, Yu JY, Liu JW, et al. Effect of process parameters on the phase transformation behavior and tensile properties of NiTi shape memory alloys fabricated by selective laser melting. Additive Manufacturing 2020;36:101545. doi:10.1016/j.addma.2020.101545.
[14] Zhao CY, Liang HL, Luo SC, et al. The effect of energy input on reaction, phase transition and shape memory effect of NiTi alloy by selective laser melting. J Alloys Compd 2020;817:153288. doi:10.1016/j.jallcom.2019.153288.
[15] Xue L, Atli KC, Zhang C, et al. Laser powder bed fusion of defect-free NiTi shape memory alloy parts with superior tensile superelasticity. Acta Mater 2022;229:117781. doi:10.1016/j.actamat.2022.117781.
[16] Dhinakaran V, Ajith J, Fahmidha AFY, et al. Wire arc additive manufacturing (WAAM) process of nickel based superalloys - A review. Mater Today: Proc 2020;21:920–5. doi:10.1016/j.matpr.2019.08.159.
[17] Wang J, Pan Z, Yang G, et al. Location dependence of microstructure, phase transformation temperature and mechanical properties on Ni-rich NiTi alloy fabricated by wire arc additive manufacturing. Mater Sci Eng, A 2019;749:218–22. doi:10.1016/j.msea.2019.02.029.
[18] Wang J, Pan ZX, Carpenter K, et al. Comparative study on crystallographic orientation, precipitation, phase transformation and mechanical response of Ni-rich NiTi alloy fabricated by WAAM at elevated substrate heating temperatures. Materials Science and Engineering A-Structural Materials Properties Microstructure and Processing 2021;800:140307. doi:10.1016/j.msea.2020.140307.
[19] Wang J, Pan ZX, Wang YF, et al. Evolution of crystallographic orientation, precipitation, phase transformation and mechanical properties realized by enhancing deposition current for dual-wire arc additive manufactured Ni-rich NiTi alloy. Additive Manufacturing 2020;34:101240. doi:10.1016/j.addma.2020.101240.
[20] Zeng Z, Cong BQ, Oliveira JP, et al. Wire and arc additive manufacturing of a Ni-rich NiTi shape memory alloy: Microstructure and mechanical properties. Additive Manufacturing 2020;32:101051. doi:10.1016/j.addma.2020.101051.
[21] Han J, Chen XY, Zhang GY, et al. Microstructure and mechanical properties of Ni50.8Ti49.2 and Ni53Ti47 alloys prepared in situ by wire-arc additive manufacturing. J Mater Process Technol 2022;306:117631. doi:10.1016/j.jmatprotec.2022.117631.
[22] Shen J, Zeng Z, Nematollahi M, et al. In-situ synchrotron X-ray diffraction analysis of the elastic behaviour of martensite and H-phase in a NiTiHf high temperature shape memory alloy fabricated by laser powder bed fusion. Additive Manufacturing Letters 2021;1:100003. doi:10.1016/j.addlet.2021.100003.
[23] Wang ZN, Lin X, Wang LL, et al. Microstructure evolution and mechanical properties of the wire plus arc additive manufacturing Al-Cu alloy. Additive Manufacturing 2021;47:102298. doi:10.1016/j.addma.2021.102298.
[24] Sinha AK, Pramanik S, Yagati KP. WAAM of Al–Cu Alloy: Effect of cooling and remelting on grain size and mechanical properties. Trans Indian Inst Met 2023;76(5):1331–9. doi:10.1007/s12666-022-02857-2.

[25] Yu L, Chen KY, Zhang YL, et al. Microstructures and mechanical properties of NiTi shape memory alloys fabricated by wire arc additive manufacturing. J Alloys Compd 2022;892:162193. doi:10.1016/j.jallcom.2021.162193.
[26] Wang LL, Xue JX, Wang Q. Correlation between arc mode, microstructure, and mechanical properties during wire arc additive manufacturing of 316L stainless steel. Materials Science and Engineering A-Structural Materials Properties Microstructure and Processing 2019;751:183–90. doi:10.1016/j.msea.2019.02.078.
[27] Qi ZW, Qi BJ, Cong BQ, et al. Microstructure and mechanical properties of wire plus arc additively manufactured 2024 aluminum alloy components: As-deposited and post heat-treated. J Manuf Process 2019;40:27–36. doi:10.1016/j.jmapro.2019.03.003.
[28] Teshome FB, Peng B, Oliveira J, et al. Role of Pd interlayer on NiTi to Ti6Al4V laser welded joints: Microstructural evolution and strengthening mechanisms. Mater Des 2023;228:111845. doi:10.1016/j.matdes.2023.111845.
[29] Zoeram AS, Mousavi SAAA. Effect of interlayer thickness on microstructure and mechanical properties of as welded Ti6Al4V/Cu/NiTi joints. Mater Lett 2014;133:5–8. doi:10.1016/j.matlet.2014.06.141.
[30] Zhu JM, Wu HH, Wu Y, et al. Influence of Ni_4Ti_3 precipitation on martensitic transformations in NiTi shape memory alloy: γ phase transformation. Acta Mater 2021;207:116665. doi:10.1016/j.actamat.2021.116665.
[31] Oliveira JP, Shen JJ, Escobar JD, et al. Laser welding of H-phase strengthened Ni-rich NiTi-20Zr high temperature shape memory alloy. Mater Des 2021;202:109533. doi:10.1016/j.matdes.2021.109533.
[32] Nam JM, Cho GB, Ahn HJ, et al. Transformation behavior and shape memory characteristics of Ti-40Ni-10Cu(at.%) alloy ribbons. Phys Scr 2007;T129:255–60. doi:10.1088/0031-8949/2007/T129/057.
[33] Zoeram AS, Mousavi SAAA. Laser welding of Ti-6Al-4V to Nitinol. Mater Des 2014;61:185–90. doi:10.1016/j.matdes.2014.04.078.
[34] Li HF, Qiu KJ, Zhou FY, et al. Design and development of novel antibacterial Ti-Ni-Cu shape memory alloys for biomedical application. Sci Rep 2016;6:37475. doi:10.1038/srep37475.
[35] Khan MI, Pequegnat A, Zhou YN. Multiple memory shape memory alloys. Adv Eng Mater 2013;15(5):386–93. doi:10.1002/adem.201200246.
[36] Chen YT, Zhang XC, Parvez MM, et al. Fabricating TiNiCu ternary shape memory alloy by directed energy deposition via elemental metal powders. Applied Sciences-Basel 2021;11(11):4863. doi:10.3390/app11114863.
[37] Chen YT, Rios CO, McLain B, et al. TiNi-based Bi-metallic shape-memory alloy by laser-directed energy deposition. Materials (Basel) 2022;15(11):3945. doi:10.3390/ma15113945.
[38] Shamsolhodaei A, Sun Q, Wang X, et al. Effect of laser positioning on the microstructure and properties of NiTi-copper dissimilar laser welds. J Mater Eng Perform 2020;29(2):849–57. doi:10.1007/s11665-020-04637-9.
[39] Yang Y, Zhan JB, Sun ZZ, et al. Evolution of functional properties realized by increasing laser scanning speed for the selective laser melting fabricated NiTi alloy. J Alloys Compd 2019;804:220–9. doi:10.1016/j.jallcom.2019.06.340.
[40] Yi XY, Gao WH, Wang HZ, et al. Dependence of aging parameters on precipitation behavior, martensitic transformation and mechanical properties of the aged Ni-Ti alloy under super high pressure. Materials Science and Engineering A-Structural Materials Properties Microstructure and Processing 2018;736:354–63. doi:10.1016/j.msea.2018.09.019.
[41] Zhou Q, Hayat MD, Chen G, et al. Selective electron beam melting of NiTi: Microstructure, phase transformation and mechanical properties. Materials Science and Engineering A-Structural Materials Properties Microstructure and Processing 2019;744:290–8. doi:10.1016/j.msea.2018.12.023.